Letter

Solution-Processed Layered Gallium Telluride Thin-Film Photodetectors

Joohoon Kang, Vinod K. Sangwan, Hong-Sub Lee, Xiaolong Liu, and Mark C Hersam

ACS Photonics, **Just Accepted Manuscript** • DOI: 10.1021/acsphotonics.8b01066 • Publication Date (Web): 25 Sep 2018

Solution-Processed Layered Gallium Telluride Thin-Film Photodetectors

Joohoon Kang[1], Vinod K. Sangwan[1], Hong-Sub Lee[1], Xiaolong Liu[2], and Mark C. Hersam[1,2,3,4]*

[1]Department of Materials Science and Engineering, Northwestern University, Evanston, IL 60208
[2]Graduate Program in Applied Physics, Northwestern University, Evanston, IL 60208
[3]Department of Chemistry, Northwestern University, Evanston, IL 60208
[4]Department of Electrical Engineering and Computer Science, Northwestern University, Evanston, IL 60208

*Correspondence should be addressed to m-hersam@northwestern.edu

ABSTRACT

Using scalable solution processing, layered gallium telluride (GaTe) nanoflake dispersions are produced in surfactant-free, low-boiling-point, water-ethanol co-solvent mixtures. During exfoliation, chemical degradation of the ambient-reactive GaTe crystals is minimized by using deoxygenated solvents in a sealed tip ultrasonication system. The structural and chemical integrity of the solution-processed GaTe nanoflakes is subsequently confirmed with a comprehensive suite of microscopic and spectroscopic analyses. Furthermore, field-effect transistors and phototransistors based on individual solution-processed GaTe nanoflakes show electronic and optoelectronic properties, respectively, that are comparable to micromechanically exfoliated GaTe. Minimal solution-processing residues from the surfactant-free, low-boiling-point co-solvent dispersion medium coupled with the high intrinsic hole doping of GaTe produces the highest electrical conductivity among solution-processed layered nanoflake thin films without post-treatment. Large-area photodetectors based on these electrically percolating thin films of solution-processed GaTe nanoflakes show a positive correlation between

responsivity and illumination intensity, with a high photoconversion gain that is explained by a combination of defect-mediated optical processes and photothermal effects. Overall, this study establishes solution-processed layered GaTe nanoflakes as a leading candidate for high-performance, large-area, thin-film photodetectors.

KEYWORDS: gallium telluride; two-dimensional; liquid phase exfoliation; anhydrous; transistor; photodetector

Layered III-VI monochalcogenides such as indium selenide (InSe)[1-3] and gallium telluride (GaTe)[4,5] have emerged as leading successors to transition metal dichalcogenides (TMDCs) for high-performance optoelectronics due to their superlative electronic and optical properties.[6] Bulk GaTe possesses a direct bandgap of ~1.7 eV and shows *p*-type electrical characteristics,[4] which places it in a relatively select group of *p*-type layered semiconductors that includes black phosphorus[7-10] and tungsten diselenide (WSe_2).[11] Like other layered materials, GaTe nanoflakes consist of covalently bonded layers that weakly interact *via* van der Waals interactions in the out-of-plane direction. However, unlike many other III-VI layered compounds, only two-thirds of the Ga-Ga bonds are perpendicular to the layers, resulting in distinctive optoelectronic properties (*e.g.*, GaTe possesses a direct bandgap in contrast to the indirect bandgaps of GaS and GaSe).[4,12,13] In addition, while TMDCs such as molybdenum disulfide (MoS_2) show a transition from indirect bandgap in the bulk to direct bandgap in the monolayer limit,[14-16] GaTe possesses a direct bandgap for all thicknesses, which provides advantages in optoelectronic and photonic applications.[4]

Despite these intrinsic optoelectronic property advantages, GaTe nanoflakes show chemical instability in ambient conditions that has hindered application development.[17,18] Although micromechanically exfoliated flakes under controlled environments have enabled initial fundamental studies of GaTe,[4,5] this approach lacks scalability for large-area applications such as thin-film photodetectors. In contrast, liquid phase exfoliation (LPE) has been previously demonstrated as a viable route for scalable processing of ambient-reactive layered nanomaterials such as black phosphorus and InSe in either anhydrous organic solvents or deoxygenated solvent systems.[2,8,9,19,20] Commonly, LPE is performed with high-boiling-point organic solvents (*e.g.*, *N*-methyl-2-pyrrolidone or dimethylformamide) that possess well-matched solubility parameters

and surface tensions (γ = ~40 mJ/m^2) that promote dispersion stability of layered nanomaterials.[21-24] Alternatively, layered nanomaterials can be exfoliated and stabilized in aqueous solutions containing amphiphilic surfactants.[14,22,23] However, residual high-boiling-point solvents or surfactants from these LPE approaches compromise flake-to-flake and flake-to-electrode contacts, particularly in percolating thin films, thus necessitating subsequent post-processing such as high-temperature annealing that is not compatible with chemically unstable nanomaterials.[2] To overcome these limitations, binary low boiling point co-solvent systems have been reported to stabilize layered materials.[2,25] The mixture of two poor solvents, water (γ = ~73 mJ/m) and ethanol (γ = ~22 mJ/m), can effectively disperse layered materials since the overall surface energy and solubility parameters are tunable based on their ratio. However, relatively few reports provide evidence of high-performance solid-state device applications that exploit the benefits of residue-free co-solvent processing.[2,25]

Here, we present a scalable method for preparing layered GaTe nanoflakes in surfactant-free, low-boiling-point, water-ethanol co-solvent mixtures. GaTe is exfoliated in a low boiling point water-ethanol mixture without further additives to minimize processing residues. Chemical degradation is further avoided by utilizing a deoxygenated solvents and employing a sealed tip ultrasonication setup. The structure, chemistry, and optical properties of the GaTe nanoflakes are then characterized through a comprehensive suite of microscopic and spectroscopic analysis methods. The resulting solution-processed individual GaTe nanoflakes show superlative electronic and optoelectronic properties that are comparable to micromechanically exfoliated samples including high intrinsic hole doping and photoresponsivities as high as ~2 × 10^6 A/W. Furthermore, the combination of minimal solution-processing residues and high intrinsic hole doping of GaTe nanoflakes results in the highest electrical conductivity reported among as-

deposited layered nanoflake thin films, enabling the production of high-performance thin-film photodetectors.

Exfoliation of pristine GaTe nanoflakes with minimal solution-processing residues is achieved via LPE in surfactant-free, low-boiling-point, water-ethanol co-solvent mixtures. As schematically shown in Figure 1a, the GaTe dispersion is prepared in three major steps: (1) Ar sparging to deoxygenate the water-ethanol co-solvent mixture; (2) ultrasonication to exfoliate GaTe nanoflakes in solution; (3) centrifugation to remove large aggregates and unexfoliated crystals. This procedure results in a visibly homogeneous dispersion of GaTe nanoflakes (Figure 1b). Figure 1c provides a schematic of a GaTe bilayer, which shows a distorted network of covalently bonded Ga and Te atoms within each layer and van der Waals bonding between layers. Atomic force microscopy (AFM) images and thickness/length histograms of the GaTe nanoflakes following solution processing are provided in Figure S1. The crystallinity and optical properties of the resulting solution-processed GaTe nanoflakes are characterized using transmission electron microscopy (TEM), selective area electron diffraction (SAED), Raman spectroscopy, optical absorbance spectroscopy, and photoluminescence excitation (PLE) spectroscopy. In Figure 1d-e, a representative high-resolution TEM image with a sharp SAED pattern confirms that the GaTe nanoflakes maintain their original crystalline structure following exfoliation in solution. The Raman spectrum in Figure 1f further shows representative GaTe vibrational modes at ~126 cm^{-1}, ~141 cm^{-1}, and ~161 cm^{-1}, which correspond to double resonant B_g and A_u modes, and the B_g mode, respectively. In addition, the peak at ~90 cm^{-1} can be attributed to A_g (90.3 cm^{-1}) and B_u (91.9 cm^{-1}) vibrational modes.[4,5] From the optical absorbance spectrum, the maximum wavelength of inter-band excitation is estimated at ~710 nm based on

the extrapolated intersection of the baseline and the absorption edge (Figure 1g), in agreement with the emission peak at ~700 nm from PLE mapping (Figure 1h).[17]

To determine the influence of the co-solvent composition on GaTe nanoflake dispersion stability, samples were prepared using identical exfoliation procedures but different water to ethanol volume ratios, as shown in Figure 2a. The overall surface energy of the co-solvent mixture is tunable based on the ratio of ethanol (γ = ~22 mJ/m) and water (γ = ~73 mJ/m). The highest concentration of GaTe nanoflakes occurs at a 1:2 v/v ratio of the water-ethanol co-solvent mixture (the corresponding optical absorbance spectra are provided in Figure S2).[2,25] The chemical degradation of GaTe during solution processing is minimized by using deoxygenated solvents and a sealed tip ultrasonication system, as reported previously.[2,8,9] To confirm the chemical integrity of the resulting GaTe nanoflakes, X-ray photoelectron spectroscopy (XPS) analysis was performed, as shown in Figure 2b. The XPS spectra of GaTe processed in deoxygenated solvents match pristine GaTe with Ga3d, $Te3d_{3/2}$, and $Te3d_{5/2}$ peaks at 19.5 eV, 583.5 eV, and 572.9 eV, respectively. On the other hand, the XPS spectra of GaTe processed with unsparged solvents exhibit additional GaO_x (20.8 eV) and TeO_x (587.2 eV, and 576.6 eV) peaks, which are indicative of deleterious oxidation during processing.[26] The time frame of chemical stability for GaTe in ambient conditions has been previously established using spectroscopic characterization including optical absorbance, Raman, and photoluminescence measurements. Unlike black phosphorus that rapidly oxides within hours following ambient exposure, GaTe nanoflake degradation occurs over the timescale of several weeks.[9,17]

The electronic properties of individual solution-processed GaTe nanoflakes were probed by fabricating field-effect transistors (FETs) using electron-beam lithography. Figure 3a shows a schematic image of an individual GaTe nanoflake FET. Experimentally, GaTe nanoflakes were

deposited from solution onto a 100 nm thick ZrO_2 dielectric that was grown by atomic layer deposition (dielectric constant, $\kappa \sim 14$) on a degenerately doped Si substrate that serves as a back gate electrode. Figure 3b shows output curves of a FET with different gate biases ranging from –20 V to 20 V (GaTe nanoflake thickness ~ 65 nm; channel length ~ 300 nm; channel width ~ 600 nm). In Figure 3c, the transfer curves reveal a field-effect mobility of ~0.2 $cm^2\ V^{-1}s^{-1}$ at a drain bias (V_D) of –1 V, which compares favorably with values previously reported for micromechanically exfoliated GaTe.[4] The device is not fully turned off even at $V_G = 20$ V, which implies exceptionally high intrinsic *p*-type doping of this GaTe nanoflake. Additional FETs with GaTe nanoflake thicknesses of ~21 nm, ~35 nm, and ~58 nm could also not be fully turned off, which suggests that the GaTe doping level is at least 5×10^{18} cm^{-3} (Figure S4). Since previous results for micromechanically exfoliated GaTe showed similar charge transport behavior, high hole doping appears to be an intrinsic property of GaTe nanoflakes.[4]

The optoelectronic properties of individual solution-processed GaTe nanoflakes were characterized by exploring the FET response under photoexcitation with a variable power laser (λ_{EX} = 516 nm). From the intensity-dependent responsivity in Figure 3d, a maximum responsivity of $\sim 2 \times 10^6$ A/W is observed at a laser intensity of $\sim 10^{-6}$ W/cm^2 with V_{GS} and V_{DS} values of -20 V and –1 V, respectively. Despite its relatively low charge carrier mobility, solution-processed GaTe nanoflakes possess high responsivity values that compete favorably with previously reported photodetectors based on layered nanomaterials including InSe (10^7 A/W),[2,27] MoS_2 (880 A/W),[28] ReS_2 (10^5 A/W),[29] GaTe (10^4 A/W),[4] and In_2Se_3 (400 A/W).[30] The underlying mechanism that allows GaTe nanoflakes to provide such high-performance phototransistors is likely related to trapping of minority carriers (*i.e.*, electrons) that leads to a space charge region in the channel and majority carriers (*i.e.*, holes) being injected to maintain

charge neutrality. In addition, the short channel device dimension (L ~ 300 nm) provides a short transit time ($\tau_{tr} = L^2/\mu V_D$, where L is the channel length and μ is the hole mobility) that results in high photocurrent gain that is proportional to τ_0/τ_{tr}, where τ_0 is the recombination lifetime of photocarriers and τ_{tr} is the transit time.

The minimal residues from solution processing in surfactant-free, low-boiling-point, water-ethanol co-solvent mixtures also result in effective flake-to-flake electrical contacts that facilitate the fabrication and testing of large-area photodetectors based on percolating networks of GaTe nanoflakes (Figure 4a). In particular, a 200 nm thick GaTe thin film was formed *via* vacuum filtration on anodic aluminum oxide (AAO) membranes followed by evaporation of 50 nm thick Au electrodes. In Figure 4b, a photograph of the large-area thin-film devices is shown along with a magnified optical microscopy image of a device with a 50 μm channel length (inset). In Figure 4c, current-voltage characteristics are shown for the GaTe thin film with and without optical illumination in vacuum conditions (~1 × 10^{-5} Torr). Due to the minimal solution processing residues and the high intrinsic doping of GaTe (as determined from the individual GaTe nanoflake charge transport measurements discussed earlier), the electrical conductivity of the as-deposited and ungated GaTe thin film (~1.8 S/m) is more than 4 orders of magnitude higher than previously reported 2D material thin films.[31-36] In contrast, although TMDCs such as MoS_2 possesses higher charge carrier mobilities than GaTe, the low intrinsic doping levels of TMDCs result in thin films with relatively low conductivity in the absence of electrostatic gating.[35,37-39]

The spectral response of the GaTe thin-film photodetector (Figure S5) shows that the photocurrent (I_{pc}) decays gradually near the GaTe fundamental band edge in a manner that is consistent with the optical absorbance peak in the 600 – 800 nm range and the

photoluminescence peak position in the PLE map (Figure 1h). The absence of a sharp photocurrent peak near the fundamental band edge in Figure S5 can be explained by the non-negligible density of shallow defects states. In Figure 4d, the intensity dependence of I_{pc} is shown with a power factor of 1.5 ($I_{pc} \sim P^{1.5}$). This superlinear intensity dependence of I_{pc} also results in a positive slope of the responsivity (R_λ) for intensities higher than 0.5 W/cm^2 (Figure 4e). Possible mechanisms for the superlinear intensity dependence of I_{pc} include a two-level Shockley-Read-Hall (SRH) recombination process that has been invoked to explain similar superlinearity in MoS_2 thin films,[35,39-41] and photothermal effects that lead to superlinearity in infrared bolometers based on carbon nanotube thin films.[42] A two-level SRH process is schematically depicted in the band diagram in Figure 4f, where E^n_F, E^p_F, R, and S indicate quasi-Fermi levels for electrons and holes, mid-gap recombination, and shallow sensitizing centers, respectively. At low light intensities, quasi-Fermi level splitting does not reach the band edges and sensitizing centers near the valence band are filled with electrons, while deep level traps facilitate SRH recombination of excess carriers. As the light intensity increases, the quasi-Fermi levels approach the band edges and sensitizing centers populate with holes while recombination centers are filled with electrons. The net effect is that electrons have effectively ionized to deep level traps and overall recombination losses decrease at higher intensities. Importantly, this effect can occur concurrently with the electron trapping effect that is responsible for the high responsivity observed for individual nanoflake photodetectors at low intensities (Figure 3).

Although the two-level SRH process is consistent with the observed photoresponse, it does not rule out contributions from photothermal effects resulting from a negative temperature coefficient of resistivity (i.e., decreasing resistance with increasing temperature) that is likely to be present in percolating thin films that are dominated by hopping transport.[6] To further explore

the possibility of photothermal effects, time-dependent photocurrent measurements were performed that show bi-exponential photocurrent rise and decay time constants of 2 sec and 8 sec, respectively (Figures S6 and S7). The amplitude of the slower exponential increases with applied bias and illumination intensity (Figures S6, S7), both of which are expected to increase the temperature of the GaTe thin film, suggesting that photothermal processes at least partially contribute to the photocurrent. However, since a pure photothermal response typically results in an intensity dependence of photocurrent with an exponent larger than 2,[40] it appears that both two-level SRH processes and photothermal effects are relevant. Ultimately, these physical processes coupled with the optoelectronic properties of GaTe nanoflakes lead to a measured R_λ of 0.2 A/W at 0.8 W/cm^2 that represents the highest responsivity at high light intensities among layered nanomaterial thin-film photodetectors (Figure 4g).[2,31-36,39]

In conclusion, structurally and chemically pristine GaTe nanoflakes have been exfoliated and stabilized in surfactant-free, low-boiling-point, deoxygenated water-ethanol co-solvent mixtures in a manner that results in exceptional optoelectronic properties for both individual nanoflakes and percolating thin films. The resulting solution-processed GaTe nanoflakes show heavy *p*-type doped electrical behavior and high photoresponsivity. This high *p*-type doping coupled with minimal solution processing residues plays a favorable role in producing highly conductive percolating GaTe nanoflake thin films. The defect structure and photothermal properties of these percolating GaTe nanoflake thin films further enable large-area photodetectors that show notably high responsitvities at high light intenstities. Overall, this work establishes a scalable pathway for processing and utilizing GaTe nanoflakes in a manner that preserves its optoelectronically-active *p*-type semiconducting properties that complement the

vast library of *n*-type layered semiconductors for emerging van der Waals heterojunction applications.[13,43]

Methods

Solvent Exfoliation: Gallium telluride (GaTe) pellets were purchased from a commercial supplier (Alfa Aesar) and stored in a dark N_2 glove box. For liquid phase exfoliation experiments, a custom tip sonicator setup was prepared by piercing the plastic lid of a 50 mL conical tube with a 0.125 inch sonicator tip. Additionally, Parafilm and Teflon tape were used to further seal the lid in order to suppress ambient contamination during exfoliation. Deoxygenated water-ethanol co-solvent mixtures were prepared by sparging with ultrahigh purity Ar for at least 30 min. The GaTe pellets and 15 mL of deoxygenated co-solvent mixture with an initial concentration of 5 mg/mL were placed in this sealed conical tube with the sonicator tip in an N_2 atmosphere. The container was then connected to the sonicator (Fisher Scientific Model 500 Sonic Dismembrator) in ambient conditions, after which the GaTe pellets was exfoliated *via* ultrasonication at ~30 W for 1 hr in an ice bath. As-prepared GaTe dispersions were centrifuged at 5,000 rpm for 10 min to remove unexfoliated GaTe pellets (Avanti J-26 XP, Beckman Coulter).

Transmission Electron Microscopy (TEM): A droplet of GaTe dispersion was deposited on a holey carbon TEM grid (Ted Pella) and fully dried with an N_2 gun. The TEM grid was then loaded into the TEM sample holder within 5 min of exposure to ambient air. TEM measurements were performed with a JEOL JEM-2100 TEM at an accelerating voltage of 200 keV.

Raman Spectroscopy: Solid-state Raman spectra were obtained using a Horiba Xplora Raman/PL system with an excitation wavelength of 532 nm. The spectra were collected for 100 sec using a 50× objective with a laser power of ~0.14 mW. PL spectra for the solution sample in Fig. 1g were obtained using a Horiba Fluorolog-3 spectrofluorometer.

X-ray Photoelectron Spectroscopy (XPS): An ultrahigh vacuum (UHV) Thermo Scientific ESCALAB 250 Xi XPS system was used at a base pressure of ~5×10^{-10} Torr to gather XPS data. The XPS data had a binding energy resolution of ~0.3-0.4 eV using a monochromated Al Kα X-ray source at ~1486.7 eV (~400 μm spot size). When using charge compensation, all core levels were charge corrected to adventitious carbon at ~284.8 eV.

Electron-Beam Lithography (EBL): For single flake field-effect transistor fabrication, solution-processed GaTe was vacuum-filtered and transferred onto 100 nm ZrO_2 substrates via PDMS stamping. Contacts were then defined with EBL in PMMA using 5 nm of Cr and 40 nm of Au as the contact metals.

Charge Transport Measurements: Electrical measurements were performed in a Lakeshore CRX 4K probe station at a pressure less than 1×10^{-5} Torr at room temperature. Two Keithley 2400 Source Meter units were used to measure current-voltage characteristics. Equation (1) was used to calculate field-effect mobility:

$$\mu_{eff} = \frac{Lg_d}{WC_{ox}V_{DS}} \quad (1)$$

where L is the channel length, g_d is the transconductance, W is the channel width, C_{ox} is the gate oxide capacitance, and V_{DS} is the applied source-drain bias.

Acknowledgments

This research was primarily supported by the National Science Foundation (DMR-1505849). This work made use of the Northwestern University NUANCE Center and the

Northwestern University Micro/Nano Fabrication Facility (NUFAB), which are partially supported by the Soft and Hybrid Nanotechnology Experimental (SHyNE) Resource (NSF ECCS-1542205), the Materials Research Science and Engineering Center (NSF DMR-1720139), the State of Illinois, and Northwestern University. XRD analysis made use of the J.B. Cohen X-Ray Diffraction Facility, which is supported by the NSF MRSEC (DMR-1720139) and the Soft and Hybrid Nanotechnology Experimental (SHyNE) Resource (NSF NNCI-1542205). Raman instrumentation was funded by the Argonne-Northwestern Solar Energy Research (ANSER) Energy Frontier Research Center (DOE DE-SC0001059). Charge transport instrumentation was funded by an ONR DURIP grant (ONR N00014-16-1-3179).

Corresponding Author

*Correspondence should be addressed to: m-hersam@northwestern.edu

Author Contributions

J.K., V.K.S., and M.C.H. planned the experiments. J.K. performed solution processing and material characterization. H.-S.L. and J.K. prepared devices by electron-beam lithography and measured charge transport. V.K.S. and J.K. measured charge transport under light illumination. X.L. collected TEM and SAED data. The manuscript was written through contributions of all authors. M.C.H. supervised the project.

Present Addresses

Joohoon Kang: Department of Chemistry, University of California, Berkeley, Berkeley, CA 94720.

Hong-Sub Lee: Department of Materials Science and Engineering, Kangwon National University, Chuncheon 24341, Republic of Korea.

Supporting Information

The supporting information gives additional data and analysis including transfer characteristics of FET devices, spectrally resolved photocurrent, and time-dependent photocurrent. This document is available free of charge via the Internet at http://pubs.acs.org.

References

(1) Bandurin, D. A.; Tyurnina, A. V.; Yu, G. L.; Mishchenko, A.; Zolyomi, V.; Morozov, S. V.; Kumar, R. K.; Gorbachev, R. V.; Kudrynskyi, Z. R.; Pezzini, S.; Kovalyuk, Z. D.; Zeitler, U.; Novoselov, K. S.; Patane, A.; Eaves, L.; Grigorieva, I. V.; Fal'ko, V. I.; Geim, A. K.; Cao, Y. High electron mobility, quantum hall effect and anomalous optical response in atomically thin InSe. *Nat. Nanotechnol.* **2017**, *12*, 223.

(2) Kang, J.; Wells, S. A.; Sangwan, V. K.; Lam, D.; Liu, X.; Luxa, J.; Sofer, Z.; Hersam, M. C. Solution-based processing of optoelectronically-active indium selnide. *Adv. Mater.* **2018**, *30*, 1802990.

(3) Chang, Y. R.; Ho, P. H.; Wen, C. Y.; Chen, T. P.; Li, S. S.; Wang, J. Y.; Li, M. K.; Tsai, C. A.; Sankar, R.; Wang, W. H.; Chiu, P. W.; Chou, F. C.; Chen, C. W. Surface oxidation doping to enhance photogenerated carrier separation efficiency for ultrahigh gain indium selenide photodetector. *ACS Photonics* **2017**, *4*, 2930-2936.

(4) Liu, F.; Shimotani, H.; Shang, H.; Kanagasekaran, T.; Zolyomi, V.; Drummond, N.; Fal'ko, V. I.; Tanigaki, K. High-sensitivity photodetectors based on multilayer GaTe flakes. *ACS Nano* **2014**, *8*, 752-760.

(5) Huang, S.; Tatsumi, Y.; Ling, X.; Guo, H.; Wang, Z.; Watson, G.; Puretzky, A. A.; Geohegan, D. B.; Kong, J.; Li, J.; Yang, T.; Saito, R.; Dresselhaus, M. S. In-plane optical anisotropy of layered gallium telluride. *ACS Nano* **2016**, *10*, 8964-8972.

(6) Sangwan, V. K.; Hersam, M. C. Electronic transport in two-dimensional materials. *Annu. Rev. Phys. Chem.* **2018,** 69, 12.1-12.27.

(7) Li, L. K.; Yu, Y. J.; Ye, G. J.; Ge, Q. Q.; Ou, X. D.; Wu, H.; Feng, D. L.; Chen, X. H.; Zhang, Y. B. Black phosphorus field-effect transistors. *Nat. Nanotechnol.* **2014,** 9, 372-377.

(8) Kang, J.; Wells, S. A.; Wood, J. D.; Lee, J. H.; Liu, X.; Ryder, C. R.; Zhu, J.; Guest, J. R.; Husko, C. A.; Hersam, M. C. Stable aqueous dispersions of optically and electronically active phosphorene. *Proc. Natl. Acad. Sci. U. S. A.* **2016**, *113*, 11688-11693.

(9) Kang, J.; Wood, J. D.; Wells, S. A.; Lee, J. H.; Liu, X. L.; Chen, K. S.; Hersam, M. C. Solvent exfoliation of electronic-grade, two-dimensional black phosphorus. *ACS Nano* **2015**, *9*, 3596-3604.

(10) Kang, D. H.; Jeon, M. H.; Jang, S. K.; Choi, W. Y.; Kim, K. N.; Kim, J.; Lee, S.; Yeom, G. Y.; Park, J. H. Self-assembled layer (SAL)-based doping on black phosphorus (BP) transistor and photodetector. *ACS Photonics* **2017**, *4*, 1822-1830.

(11) Lee, C. H.; Lee, G. H.; van der Zande, A. M.; Chen, W.; Li, Y.; Han, M.; Cui, X.; Arefe, G.; Nuckolls, C.; Heinz, T. F.; Guo, J.; Hone, J.; Kim, P. Atomically thin p-n junctions with van der waals heterointerfaces. *Nat. Nanotechnol.* **2014**, *9*, 676-681.

(12) Plucinski, L.; Johnson, R. L.; Kowalski, B. J.; Kopalko, K.; Orlowski, B. A.; Kovalyuk, Z. D.; Lashkarev, G. V. Electronic band structure of GaSe(0001): Angle-resolved photoemission and *ab-initio* theory. *Phys. Rev. B* **2003,** 68, 125304.

(13) Islam, A.; Lee, J.; Feng, P. X. L. Atomic layer GaSe/MoS_2 van der waals heterostructure photodiodes with low noise and large dynamic range. *ACS Photonics* **2018**, *5*, 2693-2700.

(14) Kang, J.; Seo, J. W. T.; Alducin, D.; Ponce, A.; Yacaman, M. J.; Hersam, M. C. Thickness sorting of two-dimensional transition metal dichalcogenides via copolymer-assisted density gradient ultracentrifugation. *Nat. Commun.* **2014**, *5*, 5478.

(15) Radisavljevic, B.; Radenovic, A.; Brivio, J.; Giacometti, V.; Kis, A. Single-layer MoS_2 transistors. *Nat. Nanotechnol.* **2011**, *6*, 147-150.

(16) Wang, Q. H.; Kalantar-Zadeh, K.; Kis, A.; Coleman, J. N.; Strano, M. S. Electronics and optoelectronics of two-dimensional transition metal dichalcogenides. *Nat. Nanotechnol.* **2012**, *7*, 699-712.
(17) Fonseca, J. J.; Tongay, S.; Topsakal, M.; Chew, A. R.; Lin, A. J.; Ko, C.; Luce, A. V.; Salleo, A.; Wu, J.; Dubon, O. D. Bandgap restructuring of the layered semiconductor gallium telluride in air. *Adv. Mater.* **2016,** 28, 6465-6470.
(18) Chew, A. R.; Fonseca, J. J.; Dubon, O. D.; Salleo, A. Long-term structural evolution of an intercalated layered semiconductor. *Adv. Funct. Mater.* **2017,** 27, 1605038.
(19) Hu, G.; Jin, X.; Ali, A.; Hu, Y.; Howe, R. C. T.; Shehzad, K.; Yang, Z.; Zhu, X.; Woodward, R. I., We, T.-C.; Jussila, H.; Wu, J.-B.; Peng, P.; Tan, P.-H.; Sun, Z.; Kelleher, E. J. R.; Zhang, M.; Xu, Y.; Hasan, T. Black phosphorus ink formulation for inkjet printing of optoelectronics and photonics. *Nat. Commun.* **2017**, *8*, 278.
(20) Hanlon, D.; Backes, C.; Doherty, E.; Cucinotta, C. S.; Berner, N. C.; Boland, C.; Lee, K.; Harvey, A.; Lynch, P.; Gholamvand, Z.; Zhang, S.; Wang, K.; Moynihan, G.; Pokle, A.; Ramasse, Q. M.; McEvoy, N.; Blau, W. J.; Wang, J.; Abellan, G.; Hauke, F.; Hirsch, A.; Sanvito, S.; O'Regan, D. D.; Duesberg, G. S.; Nicolosi, V.; Coleman, J. N. Liquid exfoliation of solvent-stabilized few-layer black phosphorus for applications beyond electronics. *Nat. Commun.* **2015,** 6, 8563.
(21) Coleman, J. N.; Lotya, M.; O'Neill, A.; Bergin, S. D.; King, P. J.; Khan, U.; Young, K.; Gaucher, A.; De, S.; Smith, R. J.; Shvets, I. V.; Arora, S. K.; Stanton, G.; Kim, H. Y.; Lee, K.; Kim, G. T.; Duesberg, G. S.; Hallam, T.; Boland, J. J.; Wang, J. J.; Donegan, J. F.; Grunlan, J. C.; Moriarty, G.; Shmeliov, A.; Nicholls, R. J.; Perkins, J. M.; Grieveson, E. M.; Theuwissen, K.; McComb, D. W.; Nellist, P. D.; Nicolosi, V. Two-dimensional nanosheets produced by liquid exfoliation of layered materials. *Science* **2011**, *331*, 568-571.
(22) Nicolosi, V.; Chhowalla, M.; Kanatzidis, M. G.; Strano, M. S.; Coleman, J. N. Liquid exfoliation of layered materials. *Science* **2013**, *340*, 1420.
(23) Kang, J.; Sangwan, V. K.; Wood, J. D.; Hersam, M. C. Solution-based processing of monodisperse two-dimensional nanomaterials. *Acc. Chem. Res.* **2017**, *50*, 943-951.
(24) Hu, G. H.; Kang, J.; Ng, L. W. T.; Zhu, X. X.; Howe, R. C. T.; Jones, C. G.; Hersam, M. C.; Hasan, T. Functional inks and printing of two-dimensional materials. *Chem. Soc. Rev.* **2018,** 47, 3265-3300.
(25) Zhou, K. G.; Mao, N. N.; Wang, H. X.; Peng, Y.; Zhang, H. L. A mixed-solvent strategy for efficient exfoliation of inorganic graphene analogues. *Angew. Chem. Int. Ed.* **2011**, *50*, 10839-10842.
(26) Balitskii, O. A.; Jaegermann, W. XPS study of InTe and GaTe single crystals oxidation. *Mater. Chem. Phys.* **2006,** 97, 98-101.
(27) Yang, H. W.; Hsieh, H. F.; Chen, R. S.; Ho, C. H.; Lee, K. Y.; Chao, L. C. Ultraefficient ultraviolet and visible light sensing and ohmic contacts in high-mobility InSe nanoflake photodetectors fabricated by the focused ion beam technique. *ACS Appl. Mater. Interfaces* **2018,** 10, 5740-5749.
(28) Lopez-Sanchez, O.; Lembke, D.; Kayci, M.; Radenovic, A.; Kis, A. Ultrasensitive photodetectors based on monolayer MoS_2. *Nat. Nanotechnol.* **2013**, *8*, 497-501.
(29) Liu, E. F.; Long, M. S.; Zeng, J. W.; Luo, W.; Wang, Y. J.; Pan, Y. M.; Zhou, W.; Wang, B. G.; Hu, W. D.; Ni, Z. H.; You, Y. M.; Zhang, X. A.; Qin, S. Q.; Shi, Y.; Watanabe, K.; Taniguchi, T.; Yuan, H. T.; Hwang, H. Y.; Cui, Y.; Miao, F.; Xing, D. Y. High responsivity

phototransistors based on few-layer ReS_2 for weak signal detection. *Adv. Func. Mater.* **2016**, *26*, 1938-1944.
(30) Jacobs-Gedrim, R. B.; Shanmugam, M.; Jain, N.; Durcan, C. A.; Murphy, M. T.; Murray, T. M.; Matyi, R. J.; Moore, R. L.; Yu, B. Extraordinary photoresponse in two-dimensional In_2Se_3 nanosheets. *ACS Nano* **2014**, *8*, 514-521.
(31) Hu, X.; Zhang, X. D.; Liang, L.; Bao, J.; Li, S.; Yang, W. L.; Xie, Y. High-performance flexible broadband photodetector based on organolead halide perovskite. *Adv. Func. Mater.* **2014**, *24*, 7373-7380.
(32) Li, J. T.; Naiini, M. M.; Vaziri, S.; Lemme, M. C.; Ostling, M. Inkjet printing of MoS_2. *Adv. Func. Mater.* **2014**, *24*, 6524-6531.
(33) Guo, F. W.; Xiao, Z. G.; Huang, J. S. Fullerene photodetectors with a linear dynamic range of 90 dB enabled by a cross-linkable buffer layer. *Adv. Opt. Mater.* **2013**, *1*, 289-294.
(34) Zhang, W. J.; Huang, J. K.; Chen, C. H.; Chang, Y. H.; Cheng, Y. J.; Li, L. J. High-gain phototransistors based on a CVD MoS_2 monolayer. *Adv. Mater.* **2013**, *25*, 3456-3461.
(35) Cunningham, G.; Khan, U.; Backes, C.; Hanlon, D.; McCloskey, D.; Donegan, J. F.; Coleman, J. N. Photoconductivity of solution-processed MoS_2 films. *J. Mater. Chem. C* **2013**, *1*, 6899-6904.
(36) McManus, D.; Vranic, S.; Withers, F.; Sanchez-Romaguera, V.; Macucci, M.; Yang, H.; Sorrentino, R.; Parvez, K.; Son, S. K.; Iannaccone, G.; Kostarelos, K.; Fiori, G.; Casiraghi, C. Water-based and biocompatible 2D crystal inks for all-inkjet-printed heterostructures. *Nat. Nanotechnol.* **2017**, *12*, 343-350.
(37) Jariwala, D.; Sangwan, V. K.; Late, D. J.; Johns, J. E.; Dravid, V. P.; Marks, T. J.; Lauhon, L. J.; Hersam, M. C. Band-like transport in high mobility unencapsulated single-layer MoS_2 transistors. *Appl. Phys. Lett.* **2013**, *102*, 173107.
(38) Kelly, A. G.; Hallam, T.; Backes, C.; Harvey, A.; Esmaeily, A. S.; Godwin, I.; Coelho, J.; Nicolosi, V.; Lauth, J.; Kulkarni, A.; Kinge, S.; Siebbeles, L. D. A.; Duesberg, G. S.; Coleman, J. N. All-printed thin-film transistors from networks of liquid-exfoliated nanosheets. *Science* **2017**, *356*, 69-72.
(39) Cunningham, G.; Hanlon, D.; McEvoy, N.; Duesberg, G. S.; Coleman, J. N. Large variations in both dark- and photoconductivity in nanosheet networks as nanomaterial is varied from MoS_2 to WTe_2. *Nanoscale* **2015**, *7*, 198-208.
(40) Bube, R. H.: *Photoelectronic properties of semiconductors*; Cambridge University Press: Cambridge, 1992.
(41) Finn, D. J.; Lotya, M.; Cunningham, G.; Smith, R. J.; McCloskey, D.; Donegan, J. F.; Coleman, J. N. Inkjet deposition of liquid-exfoliated graphene and MoS_2 nanosheets for printed device applications. *J. Mater. Chem. C* **2014,** 2, 925-932.
(42) Itkis, M. E.; Borondics, F.; Yu, A. P.; Haddon, R. C. Bolometric infrared photoresponse of suspended single-walled carbon nanotube films. *Science* **2006**, *312*, 413-416.
(43) Ye, L.; Li, H.; Chen, Z. F.; Xu, J. B. Near-infrared photodetector based on MoS_2/black phosphorus heterojunction. *ACS Photonics* **2016**, *3*, 692-699.

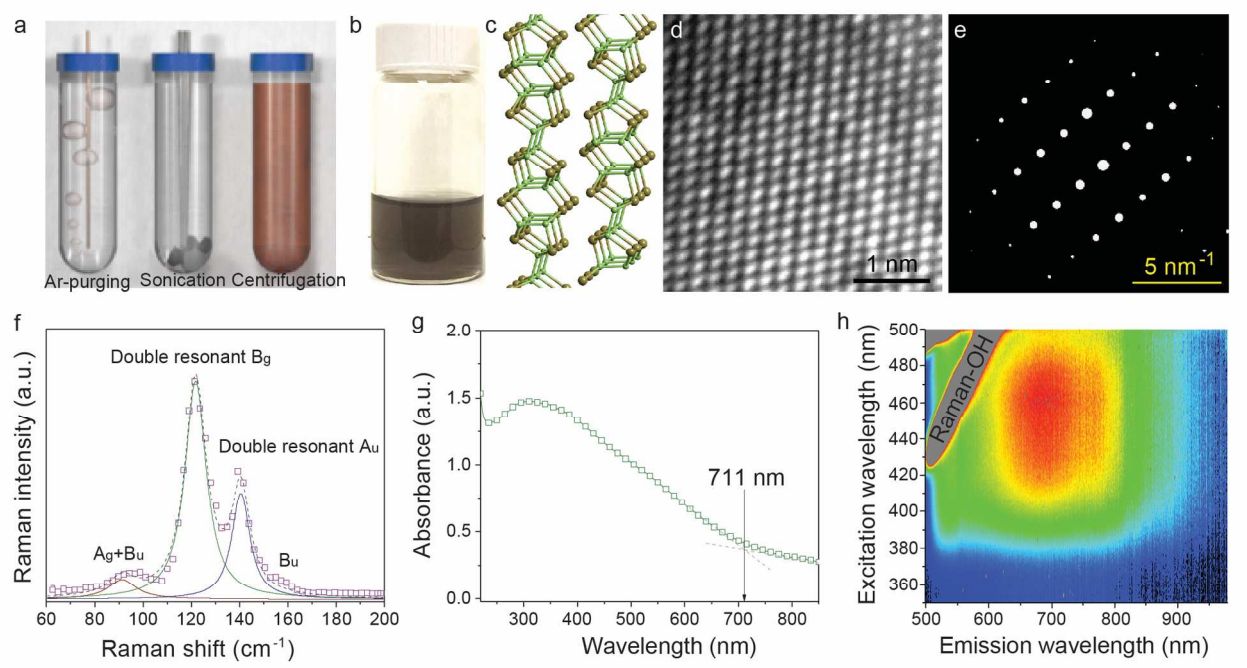

Figure 1. Characterization of GaTe nanoflakes processed in surfactant-free, low-boiling-point, water-ethanol co-solvent mixtures. (a) A schematic of the GaTe nanoflake dispersion preparation steps that minimize exposure to ambient air during processing. (b) Photograph of a GaTe dispersion in a water-ethanol co-solvent mixture after ultrasonication and centrifugation. (c) Schematic showing the atomic structure of layered GaTe (Ga: green, Te: brown). (d) High-resolution transmission electron microscopy (HRTEM) image of solution-processed GaTe nanoflakes. (e) Selected area electron diffraction (SAED) pattern of solution-processed GaTe nanoflakes. (f) Raman spectrum of solution-processed GaTe nanoflakes. (g) Optical absorbance spectrum of a GaTe dispersion with the band-edge estimated at ~710 nm. (h) Photoluminescence excitation (PLE) map of a GaTe dispersion. The label 'Raman-OH' at the upper left corner indicates the Raman mode of water.

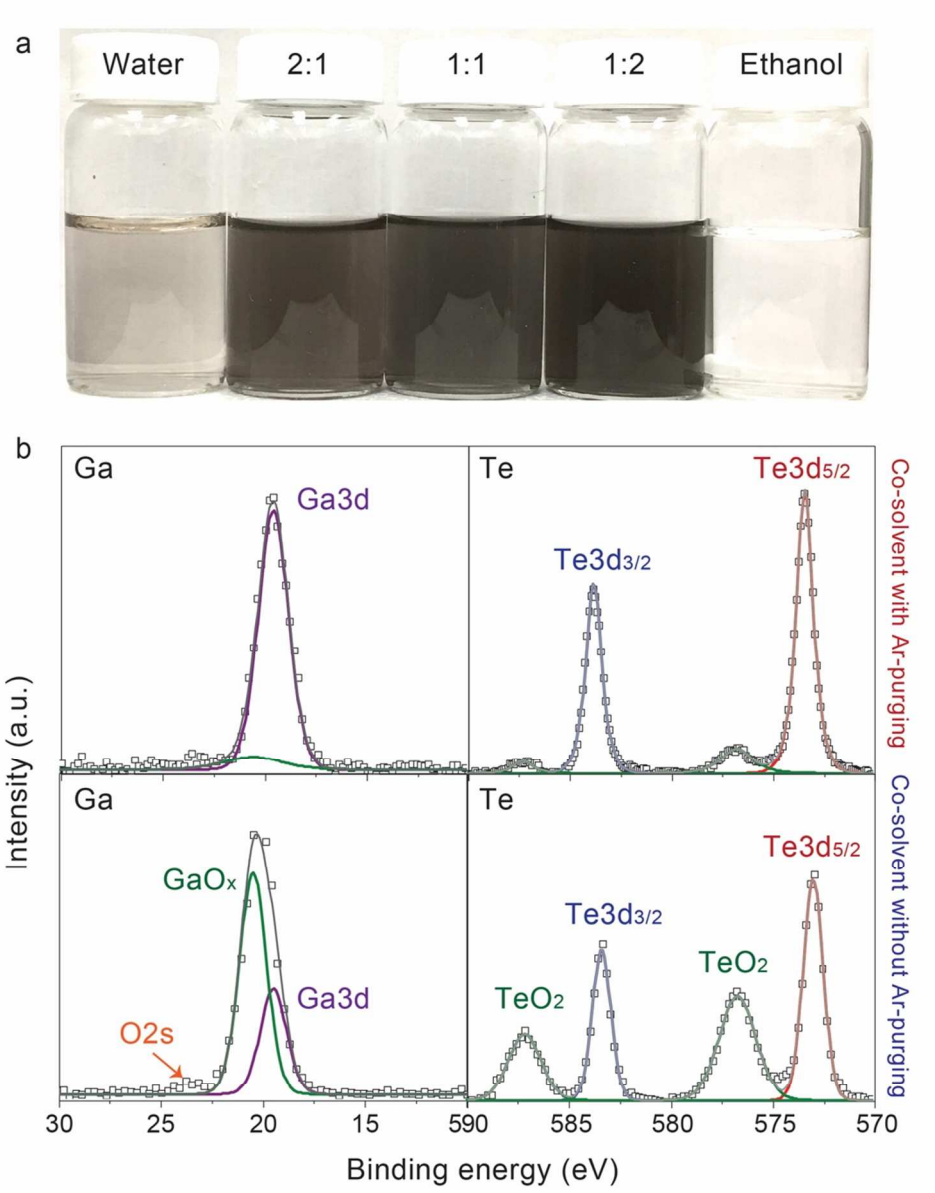

Figure 2. Stability and chemistry of GaTe nanoflake dispersions. (a) Photograph of as-prepared GaTe dispersions for different water-ethanol ratios. (b) X-ray photoelectron spectroscopy (XPS) analysis of GaTe dispersions with (top) or without (bottom) Ar sparging of the water-ethanol co-solvent mixture.

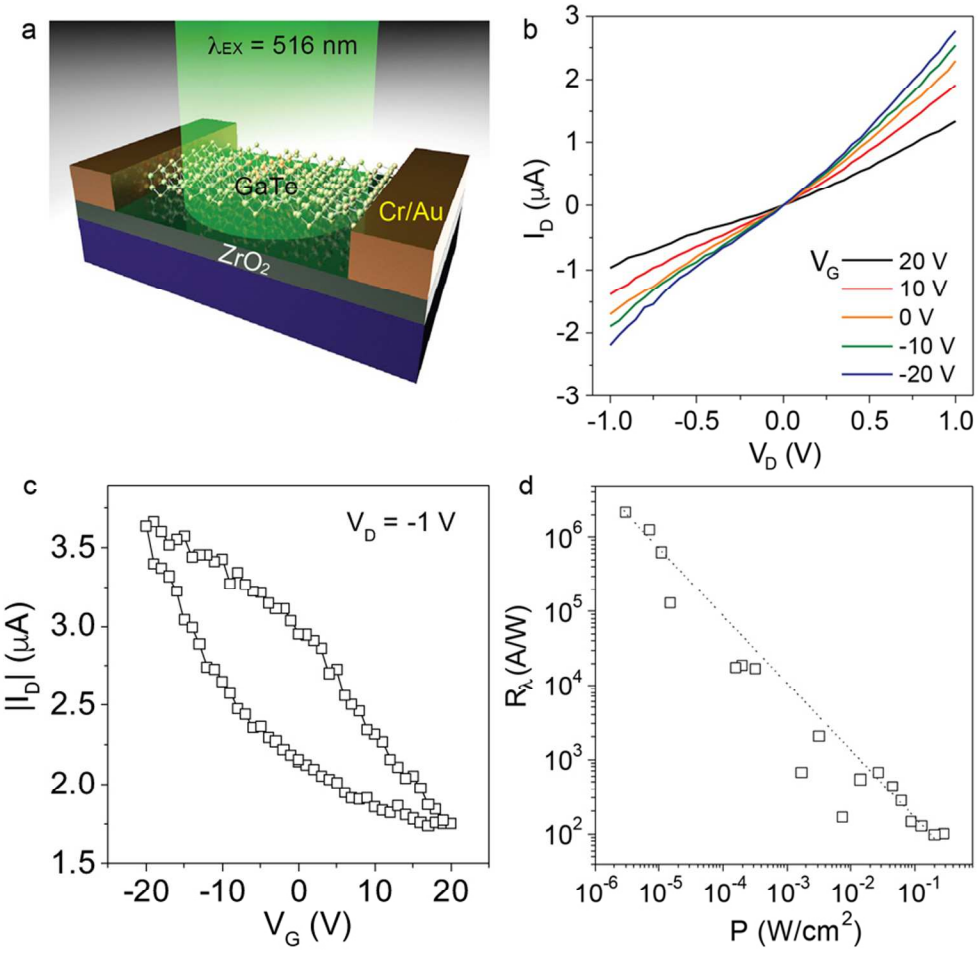

Figure 3. Electronic and optoelectronic properties of individual GaTe nanoflake devices. (a) A schematic of a GaTe nanoflake phototransistor. (b) Output characteristics of a GaTe nanoflake field-effect transistor at different gate biases (V_G). (c) Transfer characteristics of a GaTe nanoflake field-effect transistor. (d) Responsivity (R_λ) as a function of illumination intensity (P) for a GaTe nanoflake phototransistor.

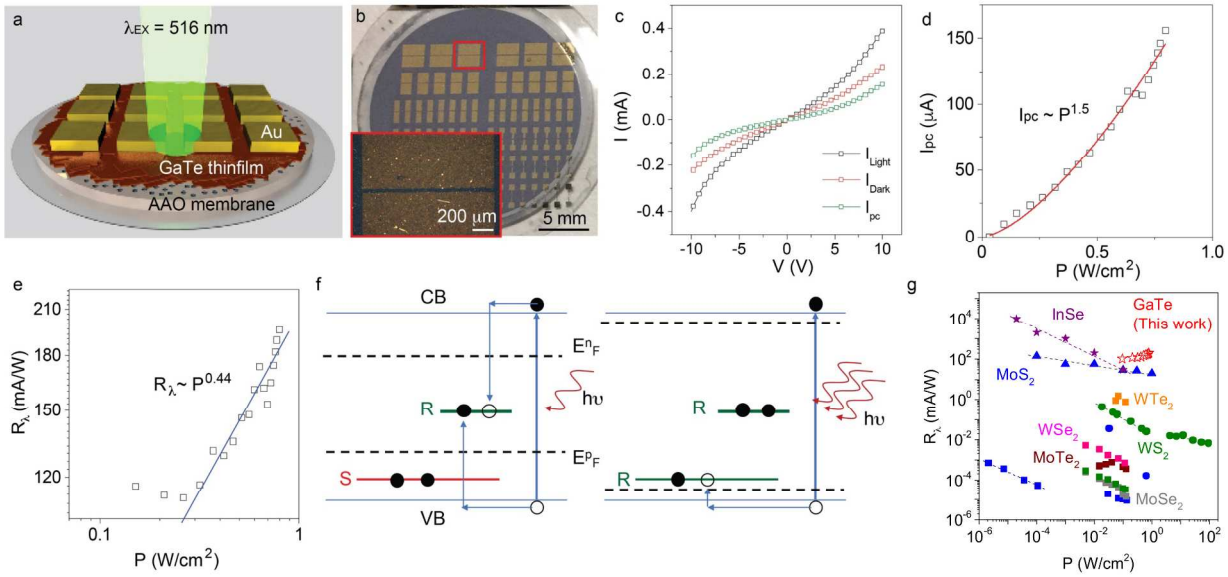

Figure 4. Optoelectronic properties of percolating GaTe nanoflake thin-film devices. (a) A schematic of an array of percolating GaTe nanoflake thin-film photodetectors. (b) A photograph of an array of percolating GaTe nanoflake thin-film photodetectors with an optical microscopy image of one device with a channel length of 50 μm (inset). (c) Current-voltage characteristics of a GaTe thin-film photodetector under vacuum in the dark (I_{Dark}, red), under illumination with a 516 nm wavelength laser with an intensity of 0.73 W/cm^2 (I_{Light}, black), and the resulting photocurrent ($I_{pc} = I_{Light} - I_{Dark}$, green). (d) Photocurrent (I_{pc}) as a function of laser power intensity (P) at $V = 10$ V, showing a superlinear power law dependence. (e) Intensity-dependent responsivity (R_λ) extracted from (d) and plotted on a logarithmic scale that reveals a power exponent of 0.44. (f) Band diagrams for the photocurrent mechanism at low (left) and high (right) laser intensities. (g) A comparison plot of responsivity *versus* illumination intensity for large-area layered nanomaterial thin-film photodetectors (MoS_2: blue; $MoSe_2$: gray; $MoTe_2$: wine; WS_2: green; WSe_2: pink; InSe: purple) prepared using different methods (star: vacuum filtration; triangle: chemical vapor deposition; square: Langmuir-Blodgett; circle: inkjet printing).[2,31-36,39]

[For Table of Contents Use Only]

Solution-Processed Layered Gallium Telluride Thin-Film Photodetectors

*Joohoon Kang[1], Vinod K. Sangwan[1], Hong-Sub Lee[1], Xiaolong Liu[2], and Mark C. Hersam[1,2,3,4]**

[1]Department of Materials Science and Engineering, Northwestern University, Evanston, IL 60208
[2]Graduate Program in Applied Physics, Northwestern University, Evanston, IL 60208
[3]Department of Chemistry, Northwestern University, Evanston, IL 60208
[4]Department of Electrical Engineering and Computer Science, Northwestern University, Evanston, IL 60208

*Correspondence should be addressed to m-hersam@northwestern.edu

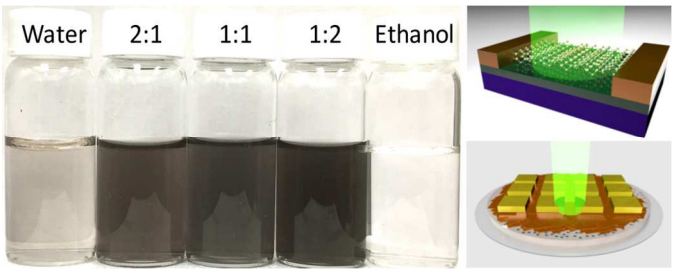

[TOC Figure – 1.375 inch x 3.5 inch]

Structurally and chemically pristine layered gallium telluride (GaTe) is stabilized in deoxygenated, surfactant-free, low-boiling-point, water-ethanol co-solvent mixtures. The resulting individual GaTe flakes exhibit superlative *p*-type doped semiconductor behavior. Minimal solution-processing residues coupled with the high intrinsic hole doping of GaTe produces the highest electrical conductivity among solution-processed layered nanoflake thin-films as well as high photoresponsivity without post-treatment.